10-21-2009

# Strategies for the Fusion of Satellite Fire Radiative Power with Burned Area Data for Fire Radiative Energy Derivation

Luigi Boschetti
*University of Maryland at College Park*

David P. Roy
*South Dakota State University*, david.roy@sdstate.edu



Recommended Citation
Boschetti, L., and D. P. Roy (2009), Strategies for the fusion of satellite fire radiative power with burned area data for fire radiative energy derivation, J. Geophys. Res., 114, D20302, doi:10.1029/2008JD011645.

# Strategies for the fusion of satellite fire radiative power with burned area data for fire radiative energy derivation

Luigi Boschetti[1] and David P. Roy[2]

Received 19 December 2008; revised 27 February 2009; accepted 6 August 2009; published 21 October 2009.

[1] Instantaneous estimates of the power released by a fire (Fire Radiative Power, FRP) are available with satellite active fire detection products. Integrating FRP in time provides an estimate of the total energy released (Fire Radiative Energy, FRE), which can be converted into burned biomass estimates needed by the atmospheric emissions modeling community. While straightforward in theory, the integration of FRP in time and space is affected by temporal and spatial undersampling imposed by the satellite sensing and orbit geometry, clouds, and active fire product omission errors. Combination of active fire FRP estimates with independently derived burned area maps provides the potential for improved and spatially explicit estimates of FRE and biomass burned. In the present work, strategies for the temporal interpolation of FRP data and for the spatial extrapolation of FRE across the burn are proposed and, as a study case, applied to an extensive grassland fire that burned for 40 days in northern Australia. The fusion of FRP estimates derived from MODIS Terra and Aqua active fire detections with the MODIS burned area product is considered, although other polar orbiting and geostationary satellite fire products could be used. Intercomparison of FRE estimated over the MODIS mapped burned area using Terra, Aqua, and Terra-Aqua combined FRP data highlights the sensitivity of FRE estimation to satellite sampling. Despite this sensitivity, FRE biomass burned estimates derived from MODIS burned area and Terra and Aqua FRP data are within 30% of regional literature estimates, suggesting that this fusion approach is a fruitful avenue for future research and validation.

**Citation:** Boschetti, L., and D. P. Roy (2009), Strategies for the fusion of satellite fire radiative power with burned area data for fire radiative energy derivation, *J. Geophys. Res.*, *114*, D20302, doi:10.1029/2008JD011645.

## 1. Introduction

[2] Estimates of atmospheric emissions due to biomass burning have conventionally been derived adopting "bottom up" inventory based methods [*Seiler and Crutzen*, 1980] as:

$$M = A \times F \times C \times E \quad (1)$$

where the quantity of emitted gas or particulate M [g] is the product of the area affected by fire A [$m^2$], the fuel loading per unit area F [g $m^{-2}$], the combustion completeness, i.e., the proportion of biomass consumed as a result of fire, C [g $g^{-1}$], and the emission factor or emission ratio, i.e., the amount of gas released per unit of biomass load consumed by the fire, E [g $g^{-1}$]. Uncertainties in these four variables propagate linearly into emissions estimates.

[3] Large area satellite burned area mapping (A) has been undertaken on a systematic basis but representative global product accuracy assessment has not been undertaken [*Roy and Boschetti*, 2009]. Fuel load (F) remains an uncertain parameter and has been variously estimated from field data, satellite data and Net Primary Production models with partitioning between fuel classes [*Van Der Werf et al.*, 2003; *Schultz et al.*, 2008]. C is a function of factors including the relative proportions of woody, grass, and leaf litter fuel, the fuel moisture and the fire behavior, which may be highly variable, for example, in African grasslands *Ward et al.* [1996] reported C as approximately 0.15 and 0.85 for smoldering and flaming combustion respectively. Emission factors (E) are largely well determined from laboratory measurements, although their temporal dynamics as a function of fuel wetness is less certain [*Hoffa et al.*, 1999; *Korontzi et al.*, 2004].

[4] An alternative satellite based methodology to derive the biomass burned [g $m^{-2}$] has been developed using time integrated instantaneous satellite measurements of the fire radiative power [*Kaufman et al.*, 1996]. The fire radiative power (FRP) [W] may be retrieved from midinfrared wavelength remotely sensed data and provides reasonably accurate (±15%) estimates of the rate of fuel consumed when combustion rates are not low (>=1 $gs^{-1}$) [*Wooster et al.*, 2005]. The total fire radiative energy (FRE) [J] released by

[1]Department of Geography, University of Maryland, College Park, Maryland, USA.
[2]Geographic Information Science Center of Excellence, South Dakota State University, Brookings, South Dakota, USA.


0148-0227/09/2008JD011645

a fire burning from time $t_1$ to $t_2$ is defined, for the ideal case of continuous FRP measurement, as:

$$FRE = \int_{t_1}^{t_2} FRP(t)dt \quad (2)$$

[5] The FRE has been shown to be linearly related to the total biomass burned [*Wooster et al.*, 2005, *Freeborn et al.*, 2008] and equation (1) can be expressed [*Wooster et al.*, 2005]:

$$M = 0.368\,10^{-3}\ FRE \times E \quad (3)$$

where the quantity of emitted gas or particulate M [g] for an active fire of given area A[$m^2$] is the product of the Fire Radiative Energy (FRE) [J] and the emission ratio E [$g\ g^{-1}$], multiplied by the coefficient 0.348 [g/J]. Thus equation (3) enables emission estimation without the need for fuel load and combustion completeness information that are not reliably defined at subregional to global scales [*French et al.*, 2004; *Wooster et al.*, 2005; *Schultz et al.*, 2008].

[6] Several issues remain for the application of equation (3) to estimate biomass burned using remotely sensed data, not least is the requirement for sufficient sampling of the FRP to capture the fire's spatiotemporal variability in order to provide reliable FRE, and so biomass burned, estimates. The FRP retrieved from satellite active fire detections is only available under relatively cloud free conditions at the time of satellite overpass [*Roberts and Wooster*, 2008]. Active fire detections from polar orbiting satellites typically under sample the temporal variability of fires due to the infrequent satellite overpass time and clouds [*Giglio*, 2007] and under sample the spatial extent of burned areas where the fire progresses rapidly across the landscape [*Roy et al.*, 2008]. Geostationary satellite active fire detections provide much improved temporal sampling (e.g., every 15 minutes for Meteosat Second Generation) over polar orbiting systems (e.g., four times a day for MODIS Terra/Aqua) but reliable geostationary active fire detection of small and cool fires is reduced due to the large pixel size and in many parts of the world the surface is sensed far from nadir and so the pixel size is large and detection accuracy reduced [*Roberts and Wooster*, 2008; *Schroeder et al.*, 2008a]. Thus locations that burned may have no active fire detection and so no FRP estimate.

[7] To date, the FRE has most usually been estimated from the FRP retrieved at detected active fire locations and times by summing the FRP values multiplied by the time difference between acquisitions [*Roberts et al.*, 2005]:

$$FRE = \sum_{t_1}^{t_2} FRP_t \Delta t \quad (4)$$

where $t_1$ and $t_2$ are the times of the first and last active fire detections in a burned region defined by the active fire detections alone. The use of equation (4), which is the adaptation of equation (2) for discrete FRP measurements, is straightforward for application to geostationary satellite data with high temporal resolution and constant time difference between acquisitions, but may be problematic for application to polar orbiting satellite data, such as provided by MODIS, because of the temporal and spatial under sampling of FRP imposed by the MODIS sensing and orbit geometry. Equation (4) implicitly assumes a linear temporal change in FRP between satellite observations. It is unknown what the impact of this assumption is on satellite derived FRE. Even with 15 minute geostationary data the FRP may vary more rapidly temporally than the satellite sampling. For example, grassland fire FRP has been observed to change by an order of magnitude with the wind direction relative to the unburned fuel bed [*Smith and Wooster*, 2005]. At the scale of individual fires and burned areas, the temporal behavior of FRP is complex [*Wooster et al.*, 2005; *Roberts et al.*, 2008]. Only when the mean FRP of many fires over large areas are considered, for example, mean MODIS FRP derived over cells of the order of 1000 × 1000km [*Ichoku et al.*, 2008] or mean Meteosat Second Generation FRP derived over continental scale land cover stratifications [*Roberts et al.*, 2008], does some form of smooth temporal FRP variability become apparent. In the absence of an explicit formulation of the temporal behavior of FRP, the assumption that FRP varies linearly between satellite observations, i.e., as equation (4), is necessary for analysis of individual fires and burned areas.

[8] Fusion of remotely sensed data sensed in different ways (e.g., wave bands and times) allows for exploitation of the different sensing characteristics [*Pohl and Van Genderen*, 1998]. Here we consider the fusion of instantaneous FRP derived from MODIS active fire detections [*Giglio et al.*, 2003] with the MODIS burned area product [*Roy et al.*, 2005] to derive FRE estimates across the MODIS mapped burned area, allowing potentially for improved and spatially explicit estimates of biomass burned over FRE derived only from MODIS active fire FRP. We illustrate issues and present strategies for: (1) Temporal integration of instantaneous FRP from MODIS active fire detections to derive FRE, (2) Spatial extrapolation of FRE over the burned area, to obtain FRE for the whole burn, including areas which burn but where, because of sampling issues, there was no active fire detection and so no FRP measurement.

## 2. Materials and Methods

### 2.1. Study Area and Time Period

[9] This study focuses on an extensive burned area in the Northern Territories, Australia, located 131–133°E and 16–18°S. The burned area is located at the border between the Old Victoria Plains and Sturt Plateau ecoregions [*Thackway and Cresswell*, 1995]. The vegetation is predominantly spinifex grasses (Triodia and Plectrachne) with sparse (<10% cover) eucaliptus trees [*Geoscience Australia*, 2004]. Figures 1 and 2 (left) show the burned area detected by the MODIS global burned area product [*Roy et al.*, 2005], displayed in a rainbow color scale to illustrate the approximate day of burning, overlaid on the MODIS blue marble true color surface reflectance to provide geographic context. Figure 1 shows the immediate vicinity and Figure 2 shows only the 14675 $km^2$ burned area considered in the rest of the paper. The area burned over a period of 40 days between the end of September and the beginning of November 2002, with multiple fire fronts moving in different directions.

### 2.2. Remotely Sensed Data

#### 2.2.1. MODIS Active Fire Product

[10] The global Collection 5 MODIS 1 km Level 2 active fire product detects the 1 km location and time of fires that are

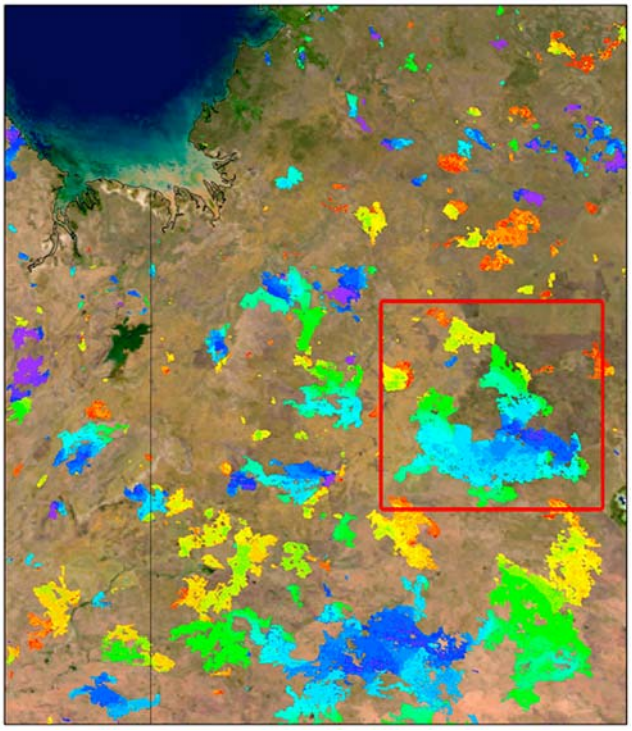

**Figure 1.** Burned areas in Northern Australia in October 2002, as detected by the MODIS global burned area product. The present study is focused on the large burned area at the center of the red rectangle. An area of approximately 6° of longitude by 7° of latitude is illustrated.

burning at the time of overpass of the NASA Terra (MOD14) and Aqua (MYD14) satellites under relatively cloud-free conditions [*Giglio et al.*, 2003]. The Level 2 product is defined in the MODIS orbit geometry, corresponding to approximately 5 minutes of sensing in the track direction, covering an area of approximately 2340 by 2030 km in the across- and along-track directions, respectively. The product contains for each 1 km pixel whether an active fire was detected (with three levels of detection confidence), or no fire detected over land, or unknown status, or cloudy, or water body. In addition, the fire radiative power [MW], band 21 (3.660–3840 $\mu$m) and band 31 (10.780–11.280 $\mu$m) blackbody temperatures [K], and average blackbody temperature in those two bands for the surrounding pixels are stored for each 1 km active fire detection.

#### 2.2.2. MODIS Global Burned Area Product

[11] The global MODIS Collection 5 burned area product (MCD45A1) is a monthly gridded 500m product that describes the approximate day of burning derived by consideration of temporal changes in reflectance and not using the MODIS active fire product [*Roy et al.*, 2005]. It is produced in the standard MODIS Land tile format in the sinusoidal projection [*Wolfe et al.*, 1998]. Each tile has fixed earth location, covering approximately 1200 × 1200 km (10° × 10° at the equator). Besides the approximate day of burning, the product describes for each pixel an extensive set of data that can be used to assess the reliability of the detection, or the presence of gaps in the time series, primarily due to cloud cover, which can affect the detection [*Roy et al.*, 2008].

### 2.3. Data Preprocessing

[12] The MOD14 and MYD14, day and night, Level 2 swath files were reprojected to the gridded 1 km Level 3 MODIS sinusoidal projection. The data were reprojected using the corresponding swath geolocation files (MOD03 and MYD03) and by nearest neighbor resampling. Reprojection and nearest neighbor resampling of the Level 2 swath FRP values results in an overestimation of observed FRP in the reprojected data. This is because the Level 2 active fire product reports the FRP for each detected fire but the ground dimensions of the MODIS Level 2 swath pixels increase with view zenith angle further from nadir [*Wolfe et al.*, 1998]. To handle this, each observed Level 2 FRP value was divided by the number of Level 3 pixels it encompassed. In this way, the total FRP in each Level 3 gridded data set is equal to the total FRP in the original Level 2 product.

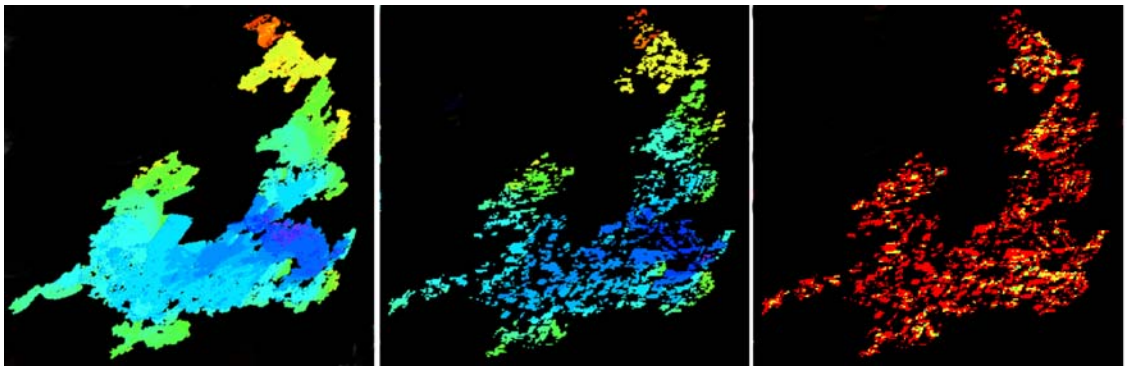

**Figure 2.** Comparison between the 500 m MODIS burned area product and the 1 km day and night active fire product for the study area in Central Australia, that burned over a 40-day period. (left) The approximate day of burning defined by the MODIS 500 m burned area product with day of burning shown in a rainbow color scale (first day blue, last day red). (middle) The date of the first detection by the MODIS 1 km active fire product, in the same color scale. (right) The number of times each pixel is detected by the MODIS active fire product (red = 1, yellow = 2, green = 3, cyan = 4). The burned area covers a total of 14,675 km$^2$, while the active fire detections cover only 5430 km$^2$.

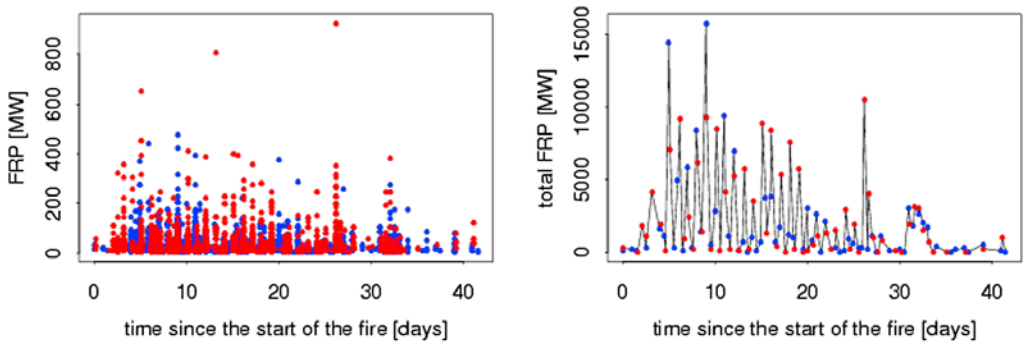


**Figure 3.** FRP time series for the active fires illustrated in the middle column of Figure 2. (left) FRP of the individual active fire detections. (right) Sum of FRP values occurring in each MODIS overpass. Red dots are Aqua and blue are Terra detections. The burning started on 22 September 2002.

### 2.4. Spatial and Temporal Sampling Issues in the Integration of Fire Radiative Power to Derive Fire Radiative Energy

[13] Estimation of the FRE, and so the total biomass consumed by fire, is subject to several remote sensing constraints because satellite data are available only at discrete intervals, due to the sensor and satellite orbit geometry and cloud contamination [*Giglio*, 2007; *Roy et al.*, 2008] and because the FRP is defined only for active fires that have a sufficient size and temperature to enable their detection [*Giglio et al.*, 2003]. Figure 2 exemplifies spatial and temporal sampling issues for MODIS data.

[14] Undersampling in the spatial domain is evident: compared to the whole extent of the area burned (Figure 2, left), only a subset of the pixels are detected as actively burning (Figure 2, middle) at the time of the MODIS day and night Aqua and Terra overpasses. The total extent of the burn, as detected by the MODIS burned area product (Figure 2, left), is 14675 $km^2$. About one third of the burned area had an Aqua and/or Terra active fire detection (Figure 2, middle). The total area of the Terra active fire detections is 2969 $km^2$, and the total area of the Aqua active fire detections is 3210 $km^2$, with 749 $km^2$ detected by both Aqua and Terra active fire detections and 5430 $km^2$ detected by one or both sensors.

[15] Undersampling in the temporal domain is evident in that many pixels are detected as active fires only once (Figure 2, right). Temporal sampling issues are also apparent in Figure 3 (left), which shows the FRP observations plotted as a function of time. The daytime observation times range between 9.45 and 11.10 (Terra) and 13.05 and 14.40 (Aqua), while the nighttime observation times range between 0.50 and 2.05 (Aqua) and 22.05 and 23.35 (Terra). The observation time is not constant because of the time difference between observations sensed across the MODIS track [*Wolfe et al.*, 2002] and because of the variation of the Terra and Aqua orbit overpass with latitude [*Kaufman et al.*, 2005].

### 2.5. Conventions and Basic Formulations

[16] In describing the formulation of the temporal and spatial integration strategy, the following conventions are used:

[17] • s is the sensor combination: Terra only, Aqua only, Aqua and Terra combined. s = {T, A, T + A}.

[18] • $OT_{s,x}$ is the set of overpass times by sensor combination s, at pixel x; note, MODIS Aqua and Terra observations never occur simultaneously, i.e.

[19] • $OT_{T+A} = OT_T \cup OT_A$ and $OT_T \cap OT_A = \varnothing$.

[20] • $t_{s,x,i}$ is the overpass time of the *i*th observation by sensor combination s of pixel x: $t_{s,x,i} \in OT_{s,x} = \{t_{s,x,0}, .., t_{s,x,N}\}$; where the first active fire detection occurs at $t_{i=0}$ and the last active fire detection occurs at $t_{i=N}$.

[21] • $FRP_{s,x,t}$ is the FRP observed by sensor combination s at location x at time t. $FRP_{s,x,t} > 0$ if, and only if, at pixel x there is an active fire detection by sensor s at time t; if not, $FRP_{s,x,t} = 0$.

[22] • $FRE_{s,x}$ is the FRE estimated at pixel x from the FRP observations by sensor combination s, over the duration of the fire ($t_N$).

[23] • BA is the set of pixels detected as burned by the burned area product.

[24] • $AF_{s,t}$ is the set of pixels with active fire detections at time t.

[25] • $AF_s$ is the set of pixels with at least one active fire detection, over the whole time period considered.

[26] • The number of pixels detected as burned, or with active fire detections, is given by the cardinality of the BA and AF sets: #{BA} and #{$AF_s$}.

[27] • $a_x$ is the area of pixel x. Consequently, $\sum_{x \in BA} a_x$ is the total area burned and $\sum_{x \in AF_s} a_x$ is the total area detected by the active fire product with sensor combination s.

### 2.6. Fusion – Temporal Integration

[28] The use of equation (4), may be problematic for application to satellite data, and in particular polar orbiting satellite data such as provided by MODIS, because of the temporal under sampling discussed in section 2.4. Three alternative and refined strategies for temporal integration of FRP data to derive FRE, termed T1, T2 and T3, are considered. In the absence of an explicit formulation of the temporal behavior of FRP of individual fires/burned areas, the three temporal integration strategies are based, as equation (4), on the conventional assumption that FRP varies linearly in the time interval between consecutive MODIS observations.

#### 2.6.1. Lumped Estimation – Strategy T1

[29] The active fires are assumed to originate from a single fire event (ignition source) or a number of fire events occurring at the same time (e.g., multiple lightning strikes

at different locations). The FRP values are integrated by linear temporal interpolation from the first to the last active fire detection, taking into account when the FRP values were observed. This is equivalent to the trapezoidal rule for numerical integration, and is illustrated in Figure 3 (right) which shows the sum of FRP values occurring in each MODIS overpass; the T1 FRE is equivalent to the area below the solid line and is computed as:

$$\mathrm{FRE}_s(\mathrm{T1}) = \sum_{i=0}^{N} \frac{\left(FRP_{s,AF_s,t_{s,i}} + FRP_{s,AF_s,t_{s,i+1}}\right)\left(t_{s,i+1} - t_{s,i}\right)}{2} \quad (5)$$

where $(t_{s,i+1} - t_{s,i})$ is the time difference between consecutive overpasses of the sensor combination s and $\mathrm{FRP}_{s,\mathrm{AF}_s,t}$ is the sum of the FRP values retrieved from active fires detected at time t, defined:

$$\mathrm{FRP}_{s,\mathrm{AF}_s,t} = \sum_{x \in AF_s} FRP_{s,x,t} \quad (6)$$

### 2.6.2. Cluster Level Estimation – Strategy T2

[30] For certain, usually large, burned areas there are multiple ignitions that occur at different times. It may be possible to identify these multiple events through a spatio-temporal clustering of the burned area and/or active fire data, for example, by labeling clusters as adjacent MODIS 1 km active fire detection pixels occurring no more than a specified number of pixels and days apart. Indeed, a spatio-temporal clustering approach is used in the final pass of the MODIS burned area product generation algorithm [*Roy et al.*, 2005] and has been applied to analyze MODIS active fire detections [*Loboda and Csiszar*, 2007]. The total FRE for each cluster is then estimated, as in T1, from the FRP values of the active fires belonging to each cluster c:

$$FRE_{s,c}(T2) = \sum_{i=0}^{N} \frac{\left(FRP_{s,c,t_{s,i}} + FRP_{s,c,t_{s,i+1}}\right)\left(t_{s,i+1} - t_{s,i}\right)}{2} \quad (7)$$

where:

$$\mathrm{FRP}_{\mathrm{s,c,t}} = \sum_{x \in c} FRP_{s,x,t} \quad (8)$$

[31] For the study area, the Terra only and the Aqua only detections were found to be too sparse to allow the reliable generation of clusters and consequently the T2 method was tested using only Terra and Aqua combined (T+A) active fire detections. A total of 108 clusters were identified using conservative temporal and spatial thresholds of 2 days and 2 pixels respectively. These thresholds were defined empirically, and assume that fires detected within 2 days at a maximum distance of three kilometers belong to the same fire event.

### 2.6.3. Pixel Level Estimation – Strategy T3

[32] FRP values are integrated temporally to derive the FRE at each pixel location: the trapezoid rule of integration is used assuming that the fire starts at the time of the MODIS observation immediately preceding the first fire detection, and stops at the time of the observation following the last fire detection. In this way, T3 can be applied even if the pixel is detected as an active fire by only one satellite overpass. As noted in section 2.4, at the single pixel scale most of the fires in the study area have a duration shorter than the 12 hours between consecutive overpasses (either Aqua or Terra) and are observed as actively burning only once (Figure 2, right). To avoid overestimating the duration of the fire, and so the FRE, in cloudy periods, observations labeled as cloudy by the MODIS active fire product are assumed not to be actively burning. T3 FRE is derived for each location x where an active fire is detected as:

$$\mathrm{FRE}_{s,\mathrm{x}}(\mathrm{T3}) = \sum_{i=0}^{N} \frac{\left(FRP_{s,x,t_{s,i}} + FRP_{s,x,t_{s,i+1}}\right)\left(t_{s,i+1} - t_{s,i}\right)}{2} \quad (9)$$

where $\mathrm{FRP}_{s,\mathrm{x,t}}$ is the FRP detected at pixel x at time t.

## 2.7. Fusion – Spatial Extrapolation

[33] The temporal integration strategies are refinements of the approach described by equation (4). None of them take into account the area that burned; they do not provide FRE estimates for every pixel in the burned area but rather a single FRE estimate for the set of active fires within the burn (T1), for each cluster (T2), and for individual pixels where active fire detections occurred (T3). The FRE for the burned area may be greater than these estimates when the burned area is greater than the area of the active fire detections, which is often the case for fires in low forest cover and grassland systems [*Roy et al.*, 2008]. It is not usually known how the FRE varies spatially, although variations are likely to occur if there are heterogeneous prefire conditions (e.g., fuel load, fuel type, wetness, slope) and fire behavior. Spatial extrapolation strategies that define an FRE estimate for all the MODIS mapped burned area, based on T1, T2 and T3, are described below.

### 2.7.1. Nonspatially Explicit Extrapolation – S1

[34] Strategy (S1, T1): The total FRE for all the pixels with active fire detections falling in the burned area is defined as equation (5). If the prefire conditions and fire behavior are homogeneous across the burn, then the FRE for any pixel in the burned area is constant:

$$\mathrm{FRE}_{\mathrm{s,x}}(\mathrm{S1,T1}) = FRE_s(T1)\frac{a_x}{\sum_{i \in AF_s} a_i} \quad (10)$$

The total FRE of the burned area is defined as:

$$\mathrm{FRE}_{\mathrm{s}}(\mathrm{S1,T1}) = \sum_{x \in BA} FRE_{s,x}(S1,T1) \quad (11)$$

Strategy (S1, T2): If the prefire conditions and fire behavior are homogeneous within each cluster then the pixels in a cluster c have the same FRE, expressed as:

$$\forall \mathrm{x} \in \mathrm{c}, \mathrm{FRE}_{\mathrm{T+A,x}}(\mathrm{S1,T2}) = FRE_{T+A,c}(T2)\frac{a_x}{\sum_{i \in c} a_i} \quad (12)$$

The total FRE of the burned area is derived from the n clusters falling within the burned area as:

$$\mathrm{FRE}_{\mathrm{T+A}}(\mathrm{S1,T2}) = \frac{\sum_{x\in BA} a_x}{\sum_{c\in BA} A_c} \sum_{c\in BA} \left(FRE_{T+A,c}(S1,T2)\right) \quad (13)$$

where $A_c$ is the area of cluster c, and $\sum_{c\in BA} A_c$ is the area of the n clusters falling in the burned area; note that $\sum_{c\in BA} A_c = \sum_{x\in AF_{T+A}} a_x$ because every pixel with an active fire detection belongs to a cluster, and consequently $0 < \sum_{c\in BA} A_c \leq \sum_{x\in BA} a_x$.

Strategy (S1,T3): The T3 method provides FRE estimates at pixel locations with active fire detections (9). The total FRE for the burned area is defined from the pixel locations where FRE(T3) is defined, as:

$$\mathrm{FRE}_{\mathrm{s}}(\mathrm{S1,T3}) = \frac{\sum_{x\in BA} a_x}{\sum_{x\in AF_s} a_x} \sum_{x\in AF_s} \left(FRE_{s,x}(T3)\right) \quad (14)$$

### 2.7.2. Spatially Explicit Extrapolation – S2

[35] Spatially explicit FRE estimates are derived by kriging the FRE data retrieved at individual pixels (T3) and for clusters (T2) within the burn to every MODIS mapped burned area pixel. Kriging is an established geospatial technique to interpolate a value at an unobserved location from observations at nearby locations [*Stein*, 1999]; here we used the Gstat kriging software [*Pebesma and Wesseling*, 1998] to estimate the FRE of each 1 km pixel where there was no direct FRE estimated by T2 or T3. This strategy assumes that the FRE is homogeneous within individual clusters and within individual pixels.

## 2.8. Data Analysis

[36] The different temporal and spatial extrapolation strategies were implemented using the MODIS active fire and burned area products for the study region illustrated in Figure 2. The total FRE for the active fire detections and the mean FRE per $km^2$ were computed for the temporal integration strategies as:

$$\text{Total } \mathrm{FRE}_{\mathrm{s}} = \sum_{x\in AFs} FRE_{s,x} \quad (15)$$

where $\mathrm{FRE}_{\mathrm{s,x}}$ is estimated with methods T1, T2, and T3 for MODIS sensor combination s. The mean FRE per $km^2$ was computed as the total FRE divided by the area of the pixels where active fires were detected one or more times:

$$\mu\left[FRE_{s,x}\right] = \frac{Total\ FRE_s}{\sum_{x\in AF_s} a_x} \quad (16)$$

Similarly, the total FRE and mean FRE per $km^2$ were derived for the different spatial extrapolation strategies but considering all the pixels in the MODIS mapped burned area and not just the pixels where active fires were detected one or more times, i.e., by replacing $x \in AF$ with $x \in BA$ in equations (15) and (16). The standard deviation of the FRE across the MODIS mapped burned area was also computed as:

$$\sigma\left[FRE_{s,x}\right] = \sqrt{\frac{1}{\#\{BA\}} \sum_{x\in BA} \left|\frac{FRE_{s,x}}{a_x} - \mu\left[FRE_{s,x}\right]\right|} \quad (17)$$

where the mean is computed using equation (16) and #{BA} is the number of pixels belonging to the burned area.

[37] Direct validation of the different FRE estimation strategy results is not possible at this scale due to the lack of spatially and temporally explicit independent FRE and biomass burned measurements. However, the FRE can be converted, using equation (3), to biomass burned. Contemporaneous fuel load data were not available for the study area, however, *Russell-Smith et al.* [2003] describe, for the two ecoregions covering the study area, average fuel loads of 0.78 $10^6$ kg $km^{-2}$ (Sturt Plateau) and 0.81 $10^6$ kg $km^{-2}$ (Old Victoria Plains) and suggest a 0.72 burning efficiency defined as the product of the combustion completeness and the proportion of the satellite pixel that effectively burned. Averaging the two fuel loading estimates and multiplying by 0.72 provides a reference biomass burned value of 0.57 $10^6$ kg $km^{-2}$. Comparisons between the FRE estimated biomass burned and this value were undertaken as an indirect form of evaluation.

# 3. Results and Discussion

[38] Table 1 summarizes the total FRE (equation (15)) and the mean FRE per $km^{-2}$ (equation (16)) for the active fire detections encompassed by the MODIS mapped burned area (Figure 2, middle and right) estimated using the T1, T2 and T3 temporal integration strategies. The estimates were calculated using Terra only, Aqua only, and Aqua and/or Terra detections (except for method T2, where the Terra only and Aqua only detections were too sparse in time and space to generate clusters). The FRE estimates tabulated in Table 1 are reasonably similar for the same sensor combinations (within 0.4 $10^9$ MJ) because all three temporal interpolation methods are based on a trapezoid integration of the FRP time series. The smallest and greatest total FRE estimates were for the Terra only and the Aqua only detections respectively for both the T1 (5.88–7.58 $10^9$ MJ) and the T3 (5.47–7.18 $10^9$ MJ) strategies. This is because the later overpass Aqua observations generally have a higher FRP than the Terra observations (Figure 3). This variability between sensors ($\sim$1.7 $10^9$ MJ) highlights the sensitivity of FRE estimation using MODIS FRP retrievals. Using Terra and Aqua detections together provide intermediate total FRE estimates of 6.54 $10^9$ MJ (T1), 6.23 $10^9$ MJ (T2) and 6.45 $10^9$ MJ (T3). When the mean FRE per $km^2$ is considered, the Aqua detections still provide higher mean FRE estimates than the Terra detections, but the combined Aqua and/or Terra mean FRE estimates are lower (Table 1). This is because the combined detections cover a greater area (5430 $km^2$) than the Terra only (2969 $km^2$) or Aqua only (3210 $km^2$) detections; this highlights a fundamental sensitivity of FRE estimation based only on MODIS active fire FRP retrievals, particularly when using either Aqua only or Terra only.

[39] Table 2 presents the total, mean and standard deviation (equations (15)–(17)) summary statistics of the FRE esti-

**Table 1.** Total FRE Estimated Using the T1, T2, and T3 Methods Over all the Active Fire Pixels Encompassed by the MODIS Burned Area[a]

| | Total FRE (MJ) | $\sum_{x \in AFs} a_x$ (km$^2$) | $\mu$ (MJ km$^{-2}$) |
|---|---|---|---|
| $T1_{T+A}$ | 6.54 $10^9$ | 5430 | 1.20 $10^6$ |
| $T1_T$ | 5.88 $10^9$ | 2969 | 1.98 $10^6$ |
| $T1_A$ | 7.58 $10^9$ | 3210 | 2.36 $10^6$ |
| $T2_{T+A}$ | 6.23 $10^9$ | 5430 | 1.15 $10^6$ |
| $T3_{T+A}$ | 6.45 $10^9$ | 5430 | 1.19 $10^6$ |
| $T3_T$ | 5.47 $10^9$ | 2969 | 1.84 $10^6$ |
| $T3_A$ | 7.18 $10^9$ | 3210 | 2.23 $10^6$ |

[a]The mean FRE per unit area ($\mu$) is computed for each sensor combination, by dividing the total FRE by the area of the pixels with active fires, reported in the second column.

mated applying the different spatial extrapolation strategies to all the MODIS mapped burned area. The total burned-area based FRE estimates (Table 2) are greater than the active fire based equivalents (Table 1) by more than a factor of two to nearly a factor of five, even though the mean FRE per km$^2$ are similar. This is expected given that less than one third of the MODIS burned area was detected by the Aqua and/or Terra active fire products. The large difference between the total FRE with respect to sensor combination, i.e., 17.7–34.6 $10^9$ MJ (T1), 16.8 $10^9$ MJ (T2), 17.4–32.8 $10^9$ MJ (T3) is, as in Table 1, indicative of the FRE sensitivity to the MODIS sampling. The spatially extrapolated Terra only and the Aqua only estimates are up to a factor of two higher than the spatially extrapolated Terra and Aqua combined estimates (Table 2) whereas for the temporally integrated strategy equivalents (Table 1) the Terra only and Aqua only estimates are about 20% higher (Aqua) and 20% lower (Terra) than the Terra and Aqua combined estimates. This apparent discrepancy between the results of Tables 1 and 2 is because the Aqua only and Terra only active fire detections cover a smaller area that the combined detections (second column in Table 1) while in Table 2 all the results are extrapolated to represent the FRE for the same 14675 km$^2$ area burned.

[40] The higher FRE estimates obtained using a single sensor can be explained in terms of temporal sampling of the active fires and in terms of the magnitude of the FRP at the overpass time of each satellite. As noted in section 2.5, Aqua and Terra overpasses never occur simultaneously, and as a consequence the time difference between two consecutive observations is always higher when a single sensor (A or T) is used, than when both are combined (T+A). The equations used for the lumped FRE temporal interpolation (T1) and for the pixel level FRE temporal interpolation (T3) are linear

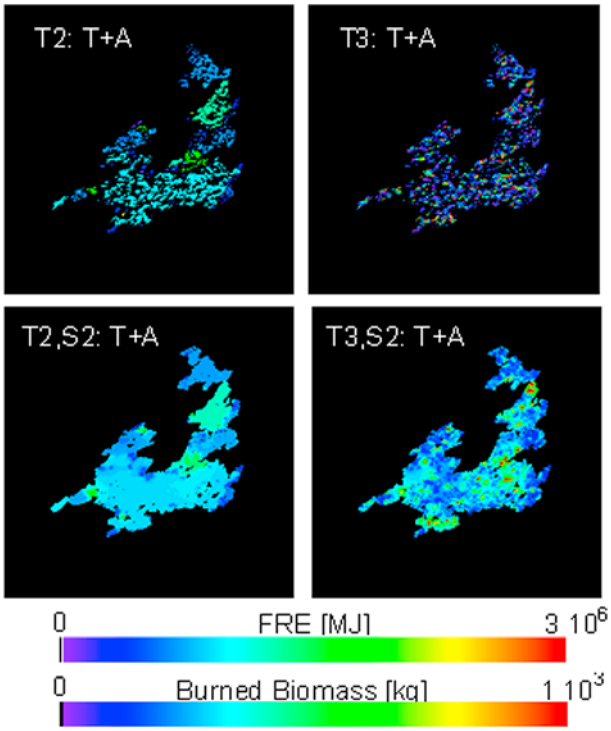


**Figure 4.** (top row) Results of the temporal interpolation by cluster (T2) and by pixel (T3). (bottom row) Results of the spatial extrapolation by kriging (S2 method) of the same data. The per pixel results are shown in terms of (top legend) FRE and (bottom legend) burned biomass per pixel.

functions of the time difference between two consecutive overpasses. Hence the FRE estimation obtained using a single sensor tends to overestimate the time interval used for the integration of the FRP observations and produces a higher FRE estimate. For this reason, the total FRE estimated from combined MODIS Aqua and Terra observations is more reliable, as more samples are available to capture the FRP in space and time. Further, the FRP at the Aqua overpass time is higher than at the Terra overpass time, which is reflected in the higher Aqua only FRE estimates than the Terra only FRE estimates (Table 2).

[41] The standard deviation FRE is always lower than the mean FRE, and the lowest standard deviation is for Terra and Aqua combined (Table 2), implying that the range of variation of the pixel FRE values is lower when both Terra and Aqua observations are used.

**Table 2.** Total FRE for the MODIS Burned Area Estimated Applying the S1 and S2 Spatial Extrapolation Methods to the Different Temporal Integration Methods[a]

| | Total FRE (MJ) (S1) | $\mu$ (MJ km$^{-2}$) (S1) | Total FRE (MJ) (S2) | $\mu$ (MJ km$^{-2}$) (S2) | $\sigma$ (MJ km$^{-2}$) (S2) |
|---|---|---|---|---|---|
| $T1_{T+A}$ | 17.7 $10^9$ | 1.20 $10^6$ | – | – | – |
| $T1_T$ | 29.0 $10^9$ | 1.98 $10^6$ | – | – | – |
| $T1_A$ | 34.6 $10^9$ | 2.36 $10^6$ | – | – | – |
| $T2_{T+A}$ | 16.8 $10^9$ | 1.15 $10^6$ | 16.8 $10^9$ | 1.14 $10^6$ | 0.20 $10^6$ |
| $T3_{T+A}$ | 17.4 $10^9$ | 1.19 $10^6$ | 17.2 $10^9$ | 1.17 $10^6$ | 0.50 $10^6$ |
| $T3_T$ | 27.0 $10^9$ | 1.84 $10^6$ | 26.3 $10^9$ | 1.79 $10^6$ | 0.77 $10^6$ |
| $T3_A$ | 32.8 $10^9$ | 2.23 $10^6$ | 32.8 $10^9$ | 2.24 $10^6$ | 1.02 $10^6$ |

[a]The mean ($\mu$) and the standard deviation ($\sigma$) FRE is computed for each sensor combination by dividing the total FRE by the area of the pixels in the MODIS burned area (14675 km$^2$).

**Table 3.** Total Biomass Burned, Mean Biomass Burned per km$^2$, and Standard Deviation Computed Using Equation (2) From the FRE Estimates Presented in Table 2

| | Total (kg) (S1) | $\mu$ (kg km$^{-2}$) (S1) | Total (kg) (S2) | $\mu$ (kg km$^{-2}$) (S2) | $\sigma$ (kg km$^{-2}$) (S2) |
|---|---|---|---|---|---|
| $T1_{T+A}$ | 6.15 $10^9$ | 0.419 $10^6$ | – | – | – |
| $T1_T$ | 10.1 $10^9$ | 0.688 $10^6$ | – | – | – |
| $T1_A$ | 12.0 $10^9$ | 0.820 $10^6$ | – | – | – |
| $T2_{T+A}$ | 5.86 $10^9$ | 0.399 $10^6$ | 5.85 $10^9$ | 0.397 $10^6$ | 0.070 |
| $T3_{T+A}$ | 6.07 $10^9$ | 0.413 $10^6$ | 5.98 $10^9$ | 0.408 $10^6$ | 0.174 |
| $T3_T$ | 9.39 $10^9$ | 0.640 $10^6$ | 9.15 $10^9$ | 0.623 $10^6$ | 0.268 |
| $T3_A$ | 1.14 $10^9$ | 0.777 $10^6$ | 1.14 $10^9$ | 0.779 $10^6$ | 0.355 |

[42] The spatially extrapolated total FRE estimated using the S1 and S2 strategies are almost the same (Table 2). This is consistent with the properties of simple kriging, which generates an unbiased estimate, i.e., the mean of the kriged data is equal to the mean of the data used as an input for the kriging. The small discrepancy between the S1 and S2 total FRE estimates is attributed to computational rounding errors. Figure 4 shows the kriged results which are discussed in more detail below.

[43] Table 3 summarizes the total and the average biomass consumed by fire obtained using the FRE estimates and equation (3). The T+A average biomass burned estimates of 0.397 $10^6$ kg km$^{-2}$ (T2,S2), 0.408 $10^6$ kg km$^{-2}$ (T3, S2), and 0.419 $10^6$ kg km$^{-2}$ (T1,S1), are within 30% of the 0.57 $10^6$ kg km$^{-2}$ reference value derived from regional fuel load and burning efficiency estimates [*Russell-Smith et al.*, 2003]. All the single sensor estimates are higher than the reference value, suggesting that their temporal sampling is insufficient, leading to an overestimation of FRE and so biomass consumed. The highest estimate (0.82 $10^6$ kg km$^{-2}$) is provided by the T1 Aqua FRE and, while likely to be overestimated, is not dissimilar to the 0.81 $10^6$ kg km$^{-2}$ Old Victoria Plains fuel load estimate. For individual pixels within the burned area, FRE and biomass burned estimates can be much smaller and much larger. Figure 4 illustrates, for Aqua and Terra, the T2 and T3 temporal interpolation FRE results (top row) and the kriged equivalents (bottom row). The T3 Terra and Aqua combined FRE estimates (Figure 4, top right quadrant) have some very high values: 8% of the pixels have FRE values that give biomass burned estimates of over $10^6$ kg km$^{-2}$, and 1% of the pixels provide burned biomass estimates over $10^7$ kg km$^{-2}$. The T2 Terra and Aqua combined FRE estimates (Figure 4, top left quadrant), are lower, and there is only one of 108 clusters providing such anomalously high burned biomass estimates. These high values may be due to sparse eucalyptus tree fires, as eucalyptus has a significantly greater calorific value than the grass [*Bowman and Wilson*, 1988]. It is unknown which of the kriged results shown on the bottom row of Figure 4 is more representative of reality. There is less spatial variability in the kriged cluster results (T2,S2) compared to the kriged pixel results (T3,S2) because of the spatial aggregation at the cluster level. These results, and the FRE standard deviations in Table 2, illustrate the spatial variability in FRE and cast doubt on the appropriateness of applying FRE estimators, such as T1 or equation (4), over large burned areas and assuming that the FRE is spatially constant.

## 4. Conclusion

[44] In this study, straightforward strategies for the fusion of fire radiative power information from the MODIS active fire product with the MODIS burned area product were presented. The strategies are based on the integration in time of instantaneous FRP estimates from the MODIS active fire product, and on the extrapolation of the resulting FRE in space to the area mapped as burned by the MODIS burned area product. A single large 14675 km$^2$predominantly grassland burned area in Northern Australia that burned for 40 days was considered. Preliminary analysis showed that the MODIS active fire detections under sampled the burning activity both in the temporal and in the spatial domain: only about a third of the pixels of the area detected as burned by the MODIS burned area product had one or more FRP measurements from the active fire product, and the majority of those pixels had only a single FRP. This under sampling is well known [*Justice et al.*, 2002; *Roy et al.*, 2005; *Giglio*, 2007; *Roy et al.*, 2008] but constrains the utility of MODIS FRP detections for derivation of FRE. Furthermore, optically thick clouds preclude active fire detection and further reduce the availability of FRP data depending on the spatiotemporal variability of clouds and satellite observations [*Roy et al.*, 2006; *Schroeder et al.*, 2008b].

[45] A number of strategies to overcome the undersampling of the fire signal were considered; all of them assume at different spatial scales (single pixels, clusters of pixels, or the entire burned area) that the FRE is constant, which may not be the case due to variations in prefire conditions and the fire behavior. Three temporal integration and two spatial extrapolation strategies were applied, repeating the analysis for different MODIS sensor combinations (Terra only, Aqua only and Terra and Aqua combined). In the absence of an independent FRE validation data set it is not possible to identify which strategy is optimal, but intercomparison of the FRE results obtained under different assumptions can be used to assess the sensitivity of the results, and gives indications for future research.

[46] The discrepancy between the FRE values obtained using the FRP measurements from a single sensor (either Terra or Aqua) and the values obtained using both Terra and Aqua highlights that FRP sampling is an important factor in reliable FRE retrieval using MODIS. The high variance of the single pixel FRE estimates points to the fact, as observed by previous workers [e.g., *Smith and Wooster*, 2005], that FRP varies instantaneously because of changes in burning conditions (e.g., wind), and so a single or small number of FRP measurements at the satellite overpass time is not representative of the FRP for the whole burning event. Use of combined MODIS Aqua and Terra FRP measurements provides more samples to capture the FRP in space and time and the limited research results indicate that their combined use provides more reliable FRE. While a validation was not possible due to lack of independent FRE and fuel consump-

tion measurements, the Aqua and Terra combined FRE estimates were plausible, providing average per km$^2$ biomass burned estimates within 30% of regional literature estimates; however, for certain pixels, and for the Terra only and particularly the Aqua only FRE, the biomass burned estimates were higher than the likely amounts of biomass present at the time of the fire.

[47] The temporal integration strategies described in the present study use active fire FRP measurements alone to derive FRE, which is the conventional approach in the literature; they do not take into account the total area that burned. The spatial extrapolation strategies we developed using the MODIS burned area product demonstrated convincingly that the FRE for the burned area was significantly greater than these active fire based estimates. This was because the burned area was greater than the area of the active fire detections, which we expect to be the case globally for fires in low forest cover and grassland systems [*Roy et al.*, 2008]. Interestingly, for the same MODIS sensor combination, all the spatial extrapolation strategies yielded similar estimates of the total burned area FRE, implying that the more simple lumped estimation strategies may be sufficient if the total FRE is the only parameter of interest. The temporal integration of satellite FRP retrievals to derive FRE assumes that the FRP varies linearly in the interval between consecutive satellite overpasses; further research is needed to study the impacts of this assumption and the temporal dynamics of FRP.

[48] The research demonstrated that there is a spatial variability of the FRE and that, through a simple kriging, it is possible to preserve such variability when extrapolating the FRE to the whole area burned. Future research will be devoted to improve the kriging. For example, *Roy et al.* [2005] demonstrated a near linear relationship between the relative change in short wave infrared reflectance and the combustion completeness multiplied by the proportion of a satellite pixel affected by fire. As the product of combustion completeness and the proportion of the pixel that burned is related directly to the biomass consumed by fire, the relative change in reflectance may provide a suitable auxiliary trend variable that could be used in the spatial extrapolation through kriging.

[49] Although this paper presents a case study for a single, albeit extensive, fire in a grassland ecosystem, the strategies described are generic and could be applied using other burned area and active fire FRP data products. As a future development, the results obtained using MODIS data will be compared to those obtained from high temporal resolution geostationary systems in tropical environments. Indeed, this fusion approach is suggested for integration of MODIS burned area data with geostationary FRP data [*Roberts and Wooster*, 2008]. Additionally, the method will be tested in conditions, such as high latitude boreal forest, where there is no coverage by geostationary systems, and where the MODIS temporal sampling issues are less severe due to the increasingly overlapping orbits further polewards [*Wolfe et al.*, 1998].

[50] **Acknowledgments.** This work was funded by NASA Earth System Science grant NNG04HZ18C and by NASA Earth Science Applications Feasibility Studies grant NNX09AO12G. Our colleague Louis Giglio is thanked for his conversations concerning the MODIS FRP product that he developed.

## References

Bowman, D. M. J. S., and B. A. Wilson (1988), Fuel characteristics of coastal monsoon forests, Northern Territory, Australia, *J. Biogeogr.*, *15*, 807–817.

Freeborn, P. H., M. J. Wooster, W. M. Hao, C. A. Ryan, B. L. Nordgren, S. P. Baker, and C. Ichoku (2008), Relationships between energy release, fuel mass loss, and trace gas and aerosol emissions during laboratory biomass fires, *J. Geophys. Res.*, *113*, D01301, doi:10.1029/2007JD008679.

French, N. H. F., P. Goovaerts, and E. S. Kasischke (2004), Uncertainty in estimating carbon estimates from boreal forest fires, *J. Geophys. Res.*, *109*, D14S08, doi:10.1029/2003JD003635.

Geoscience Australia (2004), Vegetation – Post-European Settlement (1988) Map, http://www.ga.gov.au/meta/ANZCW0703005426.html (last checked 19 December 2008)

Giglio, L. (2007), Characterization of the tropical diurnal fire cycle using VIRS and MODIS observations, *Remote Sens. Environ.*, *108*, 407–421.

Giglio, L., J. Descloitres, C. O. Justice, and Y. J. Kaufman (2003), An Enhanced Contextual Fire Detection Algorithm for MODIS, *Remote Sens. Environ.*, *87*, 273–282.

Hoffa, E., D. Ward, W. Hao, R. Susott, and R. Wakimoto (1999), Seasonality of carbon emissions from biomass burning in a Zambian savanna, *J. Geophys. Res.*, *104*, 13,841–13,853.

Ichoku, C., L. Giglio, M. J. Wooster, and L. A. Remer (2008), Global characterization of biomass-burning patterns using satellite measurements of fire radiative energy, *Remote Sens. Environ.*, *112*, 2950–2962.

Justice, C., L. Giglio, S. Korontzi, J. Owens, J. Morisette, D. Roy, J. Descloitres, S. Alleaume, F. Petitcolin, and Y. Kaufman (2002), The MODIS fire products, *Remote Sens. Environ.*, *83*, 244–262.

Kaufman, Y., L. Remer, R. Ottmar, D. Ward, L. Rong-R, R. Kleidman, R. Fraser, L. Flynn, D. McDougal, and G. Shelton (1996), Relationship between remotely sensed fire intensity and rate of emission of smoke: SCAR-C experiment, in *Global Biomass Burning*, edited by J. Levine, pp. 685–696, MIT Press, Mass.

Kaufman, Y., et al. (2005), A critical examination of the residual cloud contamination and diurnal sampling effects on MODIS estimates of aerosol over ocean, *IEEE Trans. Geosci. Remote Sens.*, *43*(12), 2886–2897.

Korontzi, S., D. P. Roy, C. O. Justice, and D. E. Ward (2004), Modeling and sensitivity analysis of fire emissions in southern African during SAFARI 2000, *Remote Sens. Environ.*, *92*, 255–275.

Loboda, T., and I. Csiszar (2007), Reconstruction of Fire Spread within wildland fire events in Northern Eurasia from the MODIS active fire product, *Global Planet. Change*, *56*(3–4), 258–273.

Pohl, C., and J. L. Van Genderen (1998), Multisensor image fusion in remote sensing: Concepts, methods and applications, *Int. J. Remote Sens.*, *19*(5), 823–854, doi:10.1080/014311698215748.

Pebesma, E. J., and C. G. Wesseling (1998), Gstat: A program for geostatistical modelling, prediction and simulation, *Comput. Geosci.*, *24*(1), 17–31.

Roberts, G. J., and M. J. Wooster (2008), Fire detection and fire characterization over Africa using Meteosat SEVIRI, *IEEE Trans. Geosci. Remote Sens.*, *46*(4), 1200–1218.

Roberts, G. J., M. J. Wooster, G. L. W. Perry, N. Drake, L.-M. Rebelo, and F. Dipotso (2005), Retrieval of biomass combustion rates and totals from fire radiative power observations: Application to southern Africa using geostationary SEVIRI imagery, *J. Geophys. Res.*, *110*, D21111, doi:10.1029/2005JD006018.

Roberts, G., M. J. Wooster, and E. Lagoudakis (2008), Annual and diurnal African biomass burning temporal dynamics, *Biogeosci. Discuss.*, *5*, 3623–3663.

Roy, D. P., and L. Boschetti (2009), Southern African validation of the MODIS, L3JRC and GlobCarbon burned area products, *IEEE Trans. Geosci. Remote Sens.*, *47*, 1032–1044, doi:10.1109/TGRS.2008.2009000.

Roy, D. P., Y. Jin, P. E. Lewis, and C. O. Justice (2005), Prototyping a global algorithm for systematic fire-affected area mapping using MODIS time series data, *Remote Sens. Environ.*, *97*, 137–162.

Roy, D. P., P. Lewis, C. Schaaf, S. Devadiga, and L. Boschetti (2006), The global impact of cloud on the production of MODIS bi-directional reflectance model based composites for terrestrial monitoring, *IEEE Geosci. Remote Sens. Lett.*, *3*, 452–456.

Roy, D. P., L. Boschetti, C. O. Justice, and J. Ju (2008), The Collection 5 MODIS burned area product: Global evaluation by comparison with the MODIS active fire product, *Remote Sens. Environ.*, *112*, 3690–3707.

Russell-Smith, J., A. C. Edwards, and G. D. Cook (2003), Reliability of biomass burning estimates from savanna fires: Biomass burning in northern Australia during the 1999 Biomass Burning and Lightning Experiment B field campaign, *J. Geophys. Res.*, *108*(D3), 8405, doi:10.1029/2001JD000787.

Schroeder, W., E. Prins, L. Giglio, I. Csiszar, C. Schmidt, J. Morisette, and D. Morton (2008a), Validation of GOES and MODIS active fire detection

products using ASTER and ETM+ data, *Remote Sens. Environ.*, *112*(5), 2711–2726.

Schroeder, W., I. Csiszar, and J. T. Morisette (2008b), Quantifying the impact of cloud obscuration on remote sensing of active fires in the Brazilian Amazon, *Remote Sens. Environ.*, *112*, 456–470.

Schultz, M. G., A. Heil, J. J. Hoelzemann, A. Spessa, K. Thonicke, J. G. Goldammer, A. C. Held, J. M. C. Pereira, and M. van het Bolscher (2008), Global wildland fire emissions from 1960 to 2000, *Global Biogeochem. Cycles*, *22*, GB2002, doi:10.1029/2007GB003031.

Seiler, W., and P. J. Crutzen (1980), Estimates of gross and net fluxes of carbon between the biosphere and the atmosphere from biomass burning, *Clim. Change*, *2*, 207–247.

Smith, A. M. S., and M. J. Wooster (2005), Remote classification of head and backfire types from MODIS fire radiative power observations, *Int. J. Wildland Fire*, *14*, 249–254.

Stein, M. L. (1999), *Interpolation of Spatial Data: Some Theory for Kriging*, Springer, New York.

Thackway, R., and I. D. Cresswell (1995), An interim biogeographic regionalisation of Australia: A framework for establishing the national systems of reserves, version 4.0, Aust. Nat. Conserv. Agency, Canberra.

Van Der Werf, G. F., J. T. Randerson, G. J. Collatz, and L. Giglio (2003), Carbon emissions from fires in tropical and subtropical ecosystems, *Global Change Biol.*, *9*(4), 547–562, doi:10.1046/j.1365-2486.2003.00604.

Ward, D. E., W. Hao, R. Susott, R. Babitt, R. Shea, J. Kaufman, and C. Justice (1996), Effect of fuel composition on combustion efficiency and emission factors for African savanna ecosystems, *J. Geophys. Res.*, *101*(D19), 23,569–23,576.

Wolfe, R., D. Roy, and E. Vermote (1998), The MODIS land data storage, gridding and compositing methodology: L2 Grid, *IEEE Trans. Geosci. Remote Sens.*, *36*, 1324–1338.

Wolfe, R., M. Nishihama, A. Fleig, J. Kuyper, D. Roy, J. Storey, and F. Patt (2002), Achieving sub-pixel geolocation accuracy in support of MODIS land science, *Remote Sens. Environ.*, *83*, 31–49.

Wooster, M. J., G. Roberts, G. Perry, and Y. J. Kaufman (2005), Retrieval of biomass combustion rates and totals from fire radiative power observations: Calibration relationships between biomass consumption and fire radiative energy release, *J. Geophys. Res.*, *110*, D24311, doi:10.1029/2005JD006318.

L. Boschetti, Department of Geography, University of Maryland, 2181 LeFrak Hall, College Park, MD 20742, USA. (luigi@hermes.geog.umd.edu)

D. P. Roy, Geographic Information Science Center of Excellence, South Dakota State University, Wecota Hall, Box 506B, Brookings, SD 57007, USA. (david.roy@sdstate.edu)